Electronic structures of GaAs/InAs(001) thin-layer systems: a tight-binding approach

1997 J. Phys.: Condens. Matter 9 6505

(http://iopscience.iop.org/0953-8984/9/31/005)

J. Phys.: Condens. Matter **9** (1997) 6505–6521. Printed in the UK PII: S0953-8984(97)79125-2

Electronic structures of GaAs/InAs(001) thin-layer systems: a tight-binding approach

Nacir Tit

Physics Department, United Arab Emirates University, PO Box 17551, Al-Ain, United Arab Emirates

Received 31 October 1996, in final form 6 March 1997

Abstract. The electronic structure of an InAs monolayer in bulk GaAs (001) is calculated in the framework of the sp^3s^* tight-binding model, which includes only nearest-neighbour interactions. The results show that both electrons and holes are localized around the inserted InAs plane, which is, therefore, playing the role of a quantum well for all charge carriers. The eigenfunctions of the confined electron and hole, calculated at the Γ point, are found to be supported by the s, p_z, and s^* orbitals of atoms in the neighbourhood of the inserted In layer, and, hence, to be confined in the *c*-axis direction, with a localization length of the order of 110 Å. In the limit of a single InAs monolayer in bulk GaAs, the energy gap is found to be 40 meV less than that of bulk GaAs. These results are in excellent agreement with the results of photoluminescence (PL) experiments, and successfully explain the observed intense PL peak, and its polarization parallel to the interface. Moreover, in a system composed of two InAs monolayers separated by *N* monolayers of GaAs, the localization of charge carriers around the InAs planes is found to decrease when *N* becomes large, as a consequence of the increase of the confinement energies. The calculated band-gap energies as a function of *N* are in reasonable agreement with the PL experimental data.

1. Introduction

The recent progress in crystal growth techniques has made it possible to grow high-quality GaAs/InAs heterostructures with abrupt interfaces. For instance, using flow-rate modulation epitaxy (FME), Sato and Horikoshi [1–3] have succeeded in synthesizing an ideal InAs monolayer in GaAs. The inserted InAs plane is found to play the role of a quantum well, which efficiently confines both electrons and holes, and produces a very sharp and intense photoluminescence (PL) peak at low temperature (2 K) [1–3]. The observed PL peak has an energy about 40 meV smaller than the GaAs bulk band-gap value. Such monomolecular-plane–host-crystal systems are attracting a great deal of interest, as they are type-I heterostructures, and, therefore, promising structures as regards high-speed and optoelectronic device applications; they are the subject of our present theoretical investigation.

In earlier experimental work [1–3], the authors fabricated structures consisting of a two-monolayer-thick layer of InAs in GaAs as well as two one-monolayer-thick layers of InAs separated by a few (say *N*) monolayers of GaAs, using the FME growth technique. They observed that the PL photon energy increases drastically with the distance between the two InAs layers, especially when *N* is small. These latter results suggest that very sharp InAs layers have been achieved using the FME growth technique, as well as a new method of band-gap engineering to be explored by varying the GaAs barrier thickness (i.e., varying

0953-8984/97/316505+17$19.50

N). The advantage of this method is that it avoids the generation of misfit dislocations due to lattice relaxation in the case of lattice-mismatched heterostructures. (We mention that our present heterostructure has a lattice mismatch of about 6.7%.) The other advantage is the artificial control of charge-carrier distributions that can be achieved.

In related work [4], we reported our *ab initio* pseudopotential calculations of the electronic structure of a single InAs monolayer in GaAs—that is, a $(GaAs)_n InAs(001)$ strained superlattice (SSL). We used a supercell of 12 atoms (i.e., $n = 5$), and an energy cut-off of 14 Ryd to simulate the InAs(GaAs) monolayer–host-crystal system. In the latter work, we adopted the valence band offset (VBO) values of 0.28 eV and 0.26 eV for the inclusion and neglect of spin–orbit effects, respectively. These VBO values [5] correspond to an interface in which the GaAs constitutes the substrate, and is lower in energy. The conduction band offset (CBO) was estimated in subsequent work [4] to be 0.62 eV (unaffected by the spin–orbit interactions), where the GaAs is higher in energy. As we were limited in our *ab initio* calculations [4] to dealing with small-size systems (such as a 12-atom supercell), while much larger systems are needed to approach the delta-doping situation, we were obliged in that work [4] to use the simple finite-square-well model to study the variation of the carrier confinement energies and the supercell energy gap versus the GaAs barrier thickness. Our results, in the case of delta doping, showed an interband transition energy 40 meV smaller than the host GaAs band gap, in good agreement with the PL experiment. Last but not least, as it is well known that the density-functional theory underestimates the band-gap energy of semiconductors and deals only with relatively small system sizes, it becomes necessary to use tight-binding models in the study of InAs(GaAs) monomolecular-plane–host-crystal systems, with special attention paid to the case of a two-monolayer-doped system.

In the present work, we employ the sp^3s^* tight-binding (TB) model to calculate the band structure and the electronic density of states of superlattices containing up to 174 atoms, and in describing the InAs(GaAs) monolayer–host-crystal structures. In the original sp^3s^* tight-binding model, suggested by Vogl *et al* [6], the inclusion of the excited s^* state successfully reproduced the unoccupied antibonding lower conduction bands as well as the occupied valence bands in semiconductors. This sp^3s^* model maintains the spirit of Harrison's model of semiconductors by constructing a nearest-neighbour tight-binding theory which preserves and displays the chemical trends. The parameters in the original model were obtained [6] by fitting the pseudopotential bands [7] while the energy gaps were fitted to the experimental values [8]. In our present work, however, we used improved empirical tight-binding parameters [9] which yielded deformation potentials in reasonable agreement with the experimental data [8], and are therefore more reliable to use for strained quantum wells. The atomic rearrangement, in this model, can successfully be described by scaling the off-diagonal elements according to the Harrison's $1/r^2$ rule [10]. However, in our present work, high-resolution electron microscopy [11] indicated that the measured interface strain is much higher than expected from the macroscopic theory of elasticity (MTE). This latter experiment showed that the InAs monolayer is strained in a configuration to conserve the bulk In–As bond length at the interface, and, therefore, it also suggested that the MTE breaks down in the monolayer limit. This observation has been corroborated by our *ab initio* calculation [4]. Hence, in our present InAs(GaAs) monolayer–host-crystal systems, the In–As bond length is kept to its bulk value.

The rest of the paper is organized as follows. In section 2, we describe the tight-binding model, and the method for calculating the electronic structures of both the bulk and the superlattices. Section 3 gives a detailed discussion of our results. The final section summarizes our main conclusions.

2. The method of calculation

The tight-binding Hamiltonian matrix elements for either bulk or tetragonal superlattice structures are expressed in terms of a basis of symmetrically orthonormalized atomic orbitals $|\mathrm{b}, \mu, \boldsymbol{R}_\mathrm{i}\rangle$, also called Löwdin orbitals [12]. Here $\boldsymbol{R}_\mathrm{i}$ denotes a Bravais lattice point referred to the unit cell, b is a basis atom in this cell, and μ denotes an orbital (such as s, p_x, p_y, p_z, or s^*) of the atom b. In reference [6] (see also appendix A), the Hamiltonian is expressed in terms of a basis $|\mathrm{b}, \mu, \boldsymbol{k}\rangle$, which is obtained via a discrete Fourier transformation of the localized orbitals $|\mathrm{b}, \mu, \boldsymbol{R}_\mathrm{i}\rangle$, given by

$$|\mathrm{b}, \mu, \boldsymbol{k}\rangle = \frac{1}{\sqrt{N_\mathrm{w}}} \sum_\mathrm{j} \mathrm{e}^{\mathrm{i}\boldsymbol{k}\cdot\boldsymbol{R}_\mathrm{j}} |\mathrm{b}, \mu, \boldsymbol{R}_\mathrm{j}\rangle \tag{1}$$

where N_w is the number of $\boldsymbol{k}$-vectors taken from within the irreducible wedge of the Brillouin zone.

The Schrödinger equation whose solutions are the Bloch functions $|n\boldsymbol{k}\rangle$ is given by

$$(H - E_{n\boldsymbol{k}})|n\boldsymbol{k}\rangle = 0 \tag{2}$$

and expressed in terms of the Löwdin basis as

$$\sum_{\mathrm{j},\nu} \left[\langle \mathrm{i}, \mu, \boldsymbol{k}|H|\mathrm{j}, \nu, \boldsymbol{k}\rangle - E_{n\boldsymbol{k}}\delta_{\mathrm{i},\mathrm{j}}\delta_{\mu,\nu}\right] \langle \mathrm{j}, \nu, \boldsymbol{k}|n\boldsymbol{k}\rangle = 0 \tag{3}$$

where n is a band index, i and j denote basis atoms, and μ and ν denote orbitals of these respective atoms. The eigenvalues, $E_{n\boldsymbol{k}}$, and the eigenvectors, $|n\boldsymbol{k}\rangle$, are obtained by means of a direct diagonalization based on the Lanczos algorithm [13] procedure. This diagonalization technique is known to be very efficient for large sparse matrices. The Hamiltonian of either the bulk fcc structure or the superlattice structure (see appendices A and B) uses the empirical tight-binding parameters given in table 1. One should emphasize, however, that in the superlattice electronic structure calculation one must take into account the band discontinuities [14]. In the tight-binding framework, the valence band offset is considered as a constant, and added to the diagonal elements of the Hamiltonian matrix (for instance, in our case, the InAs on-site energies are shifted by the VBO, since the valence band edge of this constituent is higher in energy when it forms an interface with the GaAs substrate). However, since the scope of our present work is the InAs(GaAs) monolayer–host-crystal systems, we have shifted up only the on-site energies of the In atom by VBO = 0.28 eV, in order to keep the wavefunction of the localized electron/hole state symmetric around the In monatomic layer according to the crystal symmetry (the results

Table 1. Empirical $\mathrm{sp}^3\mathrm{s}^*$ tight-binding parameters for GaAs and InAs, in units of eV, from the work of reference [9]. The same notation as in reference [6] is used. The bond lengths (d) are in Å.

Compound	d	E(s, a)	E(p, a)	E(s, c)	E(p, c)	E(s*, a)	E(s*, c)
GaAs	2.45	−8.3431	1.0414	−2.6569	3.6685	7.5412	6.7397
InAs	2.62	−9.5381	0.9099	−2.7219	3.7201	7.4099	6.7401
Compound	V(s, s)	V(x, x)	V(x, y)	V(sa, pc)	V(sc, pa)	V(s*a, pc)	V(pa, s*c)
GaAs	−6.4513	1.9546	5.0779	4.4800	5.7839	4.4378	4.8083
InAs	−5.6052	1.8398	4.4693	3.0354	5.4389	3.3744	3.9097

are displayed in the next section). Moreover, the spin–orbit effects are included only in our supercell calculations, through the values used for the band offsets.

The energy spectrum $E_{n\boldsymbol{k}}$ obtained, and the corresponding wavefunctions $|n\boldsymbol{k}\rangle$ are used to calculate the following quantities. The total density of states is given by

$$N(E) = \frac{1}{N_{\mathrm{w}}} \sum_{n,\boldsymbol{k}} \delta(E - E_{n\boldsymbol{k}}) \tag{4}$$

where N_{w} is the number of $\boldsymbol{k}$-vectors taken from within the irreducible wedge of the Brillouin zone. The local density of states due to orbital μ on atom b is given by

$$N_{\mathrm{b},\mu}(E) = \frac{1}{N_{\mathrm{w}}} \sum_{n,\boldsymbol{k}} |\langle \mathrm{b}, \mu, \boldsymbol{R}_{\mathrm{i}} | n\boldsymbol{k}\rangle|^2 \delta(E - E_{n\boldsymbol{k}}). \tag{5}$$

The local density of states due to site b is given by

$$N_{\mathrm{b}}(E) = \sum_{\mu=1}^{5} N_{\mathrm{b},\mu}(E) \tag{6}$$

and the partial density of states due to the atomic species of type α (such as Ga or As or In atoms) is given by

$$N_{\alpha}(E) = \sum_{\mathrm{b}} N_{\mathrm{b}}(E) \tag{7}$$

where the sum runs over only sites of type α.

The $\boldsymbol{k}$-space integration carried out in evaluating equations (4) and (5) is performed using the tetrahedron method [15], and the δ-function is numerically approximated to a gaussian:

$$\frac{1}{\sqrt{2\pi}\sigma} \exp\left(-\frac{(E - E_{n\boldsymbol{k}})^2}{2\sigma^2}\right)$$

of width $\sigma = 0.05$ eV. All of the total densities of states in our calculations are normalized to ten electrons (i.e., one zinc-blende molecule). The results of our calculations are presented in the next section.

3. Results and discussion

3.1. Bulk fcc structure

In figures 1 and 2, we display the electronic structures of bulk GaAs and bulk InAs respectively. These results were obtained using the ten-band (sp^3s^*) model whose parameters are given in table 1. The top of the valence band is chosen as the energy reference. The energy gaps, obtained with the neglect of spin–orbit interactions, are $E_{\mathrm{g}} = 1.55$ eV and $E_{\mathrm{g}} = 0.43$ eV for GaAs and InAs respectively (compared to the results 1.07 eV and 0.58 eV from our previous *ab initio* calculations [4], while the respective experimental values are 1.52 eV and 0.42 eV). The crystal symmetry of the zinc-blende structure belongs to the $\mathrm{T_d}$ point group (symmorphic space group), whereas the Brillouin zone is similar to that of the fcc structure, because it depends uniquely on the Bravais lattice. The special points L, Γ, X, and U (≡K) in the Brillouin zone have the respective point group symmetries $\mathrm{D_{3d}}$, $\mathrm{O_h}$, $\mathrm{D_{4h}}$, and $\mathrm{C_{2v}}$, whose respective irreducible representations have dimensionalities up to $d = 2$, 3, 2, and 1, respectively. This is consistent with the bands obtained, whose degeneracies are from 1 up to the above dimensionality d at the respective high-symmetry points. Similarly, the high-symmetry lines in the Brillouin zone, Λ (the LΓ line), Δ (the

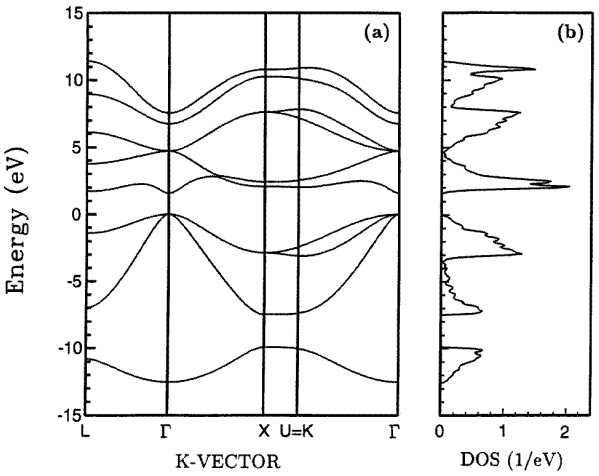

Figure 1. The electronic structure of bulk GaAs calculated using the sp^3s^* tight-binding model of reference [9]. (a) Energy bands; (b) the density of states. The top of the valence band is taken as the energy reference, and the spin–orbit interactions are excluded. The density of states is normalized to ten electrons.

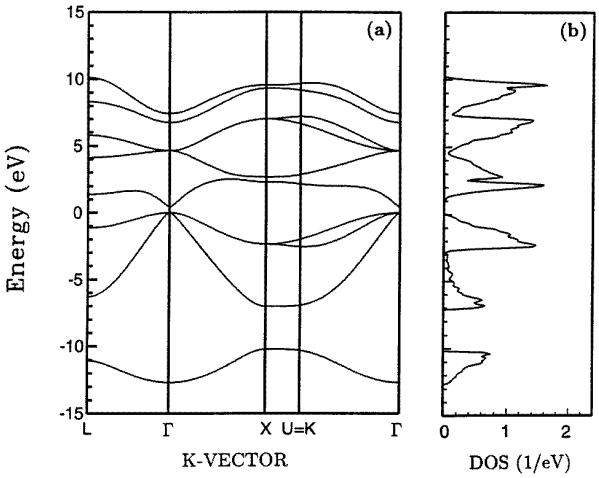

Figure 2. As figure 1, but for bulk InAs.

ΓX line), S (the XU line), and Σ (the KΓ line) have the respective point group symmetries C_{3v}, C_{4v}, C_{2v}, and C_{2v}. These groups have irreducible representations of dimensionalities up to 2, 2, 1, and 1, respectively, and these numbers correspond to the degeneracies of the bands on these high-symmetry lines. In figures 1(b) and 2(b), we display the density of states (DOS) calculated using the tetrahedron method. It consists mainly of three groups of bands. The lowest group is dominated by a contribution from the s orbitals of anion (As) atoms. The second group, which is the valence band (VB), consists of the cationic s states and all of the p states. Here, one should note two qualitative trends.

(i) In general, as the lattice constant increases, the valence band width decreases (compare figures 1(b) and 2(b)). This can be ascribed to a reduction of the hybridization with

increasing separation of the atomic constituents. Moreover, predominantly ionic materials have wider VBs than do predominantly covalent materials.

(ii) The other trend is that the optical gap in common anion (or cation) semiconductors decreases with the heavier cation (or anion).

The third group of bands, which form the conduction band (CB), are mainly due to contributions from all of the p and s^* orbitals.

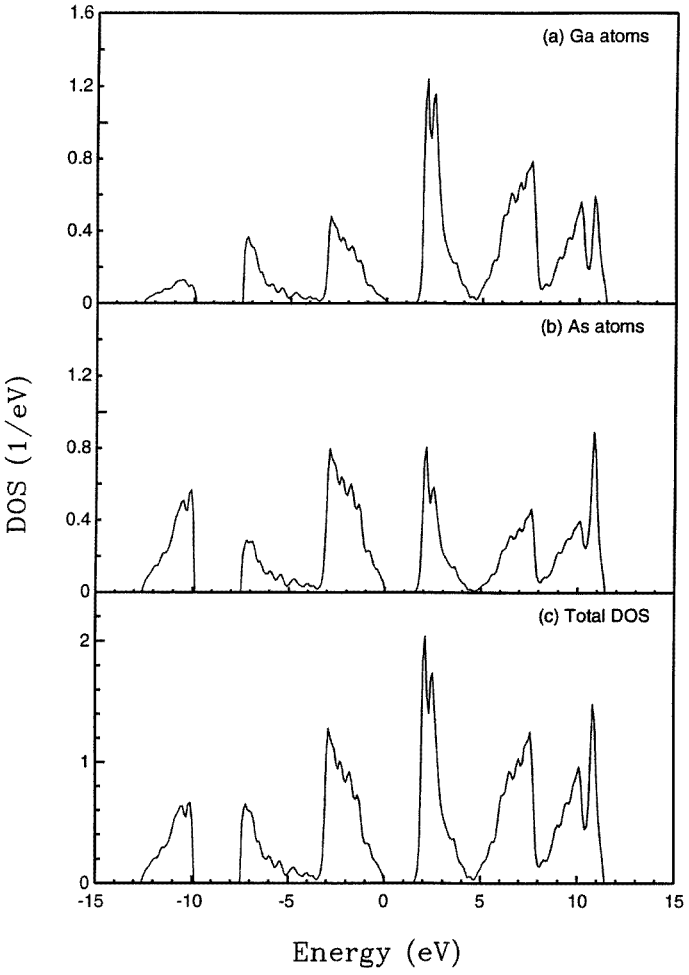

Figure 3. Partial density-of-states contributions from orbitals on (a) Ga atoms and (b) As atoms to (c) the total density of states of pure GaAs. The total DOS is normalized to ten electrons.

In figure 3, we display the total and partial densities of states for GaAs, which constitutes the substrate (host crystal) in the InAs(GaAs) monolayer–host-crystal systems. As can be seen in panels (a) and (b), Ga and As atoms experience the same point group symmetry (T_d), and, as a consequence, they have very similar splittings and DOS profiles. Note that the total DOS is normalized to ten electrons. One also may notice that most of the weight of the Ga local DOS is in the valence and lower bands, whereas the In contributes more to the conduction band structure. This reflects the fact that GaAs is a polar material.

3.2. Superlattice structure

We use the $(InAs)_1/(GaAs)_n(001)$ tetragonal superlattice model to describe the InAs(GaAs) monomolecular-plane–host-crystal system. The In–As bond length is preserved at its equilibrium bulk value (2.62 Å). The GaAs interlayer distance is 2.83 Å, while the InAs is distorted and expanded in the *c*-axis direction with an interlayer distance of 3.39 Å. First, we used a supercell similar to that studied in our previously published *ab initio* calculations [4], namely the $(GaAs)_5InAs(001)$ superlattice. We aim to explore new trends using the local and partial DOS's. We display in figure 4(a) the bands of pure GaAs, which is considered in a 12-atom supercell in order to facilitate the comparison to the strained-superlattice (SSL) bands presented in figure 4(b). Each of these two figures contains 60

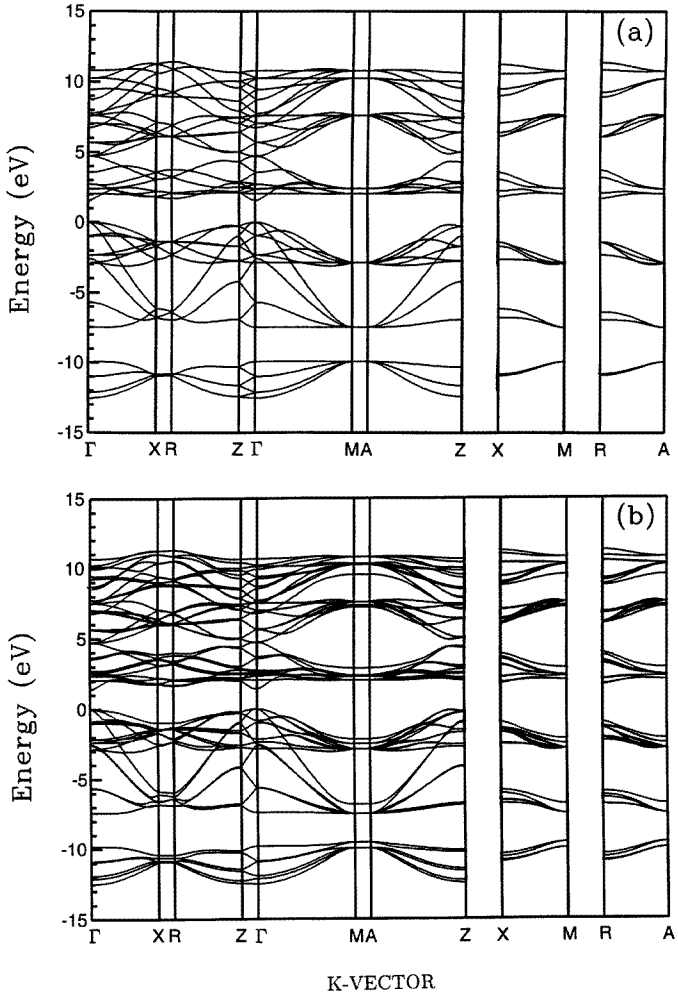

Figure 4. The nonrelativistic band structures of a 12-atom tetragonal superlattice corresponding to: (a) pure bulk GaAs; and (b) a $(GaAs)_5InAs(001)$ SSL structure. In (b), the In–As bond length is kept equal to its bulk equilibrium value. We choose to present pure GaAs in the supercell in order to facilitate the comparison with the SSL bands. The top of the valence the band is taken as the energy reference.

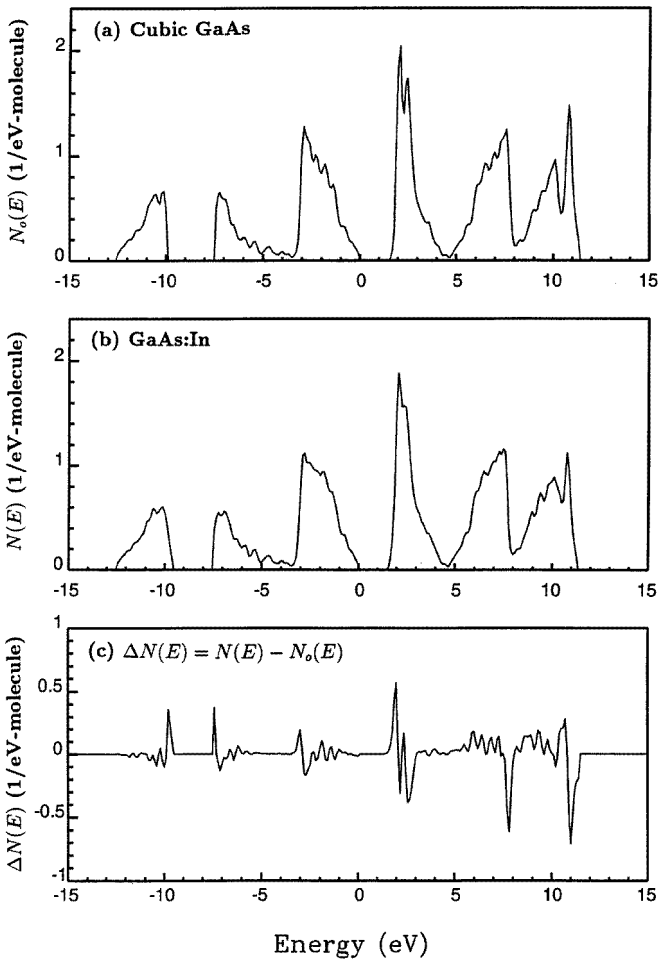

Figure 5. The densities of states $N_0(E)$ and $N(E)$ corresponding to the band structures shown in figure 4: (a) pure bulk GaAs and (b) a $(GaAs)_5InAs$ SSL. The difference of the DOS's, $\Delta N(E) = N(E) - N_0(E)$, is displayed in panel (c) to illustrate the effects of the insertion of the InAs monolayer.

bands among which 6 constitute the lower group (we suggested [4] that these 6 bands can be attributed to As atoms, but see below for further details), and 18 bands contribute to the valence band structure, while the remaining 36 bands form the conduction band. The band-gap energy is $E_g = 1.55$ eV for figure 4(a) and $E_g = 1.31$ eV for figure 4(b), without the inclusion of spin–orbit interactions. (Our previous *ab initio* [4] band gap, corresponding to the superlattice structure of figure 4(b), was underestimated to have the value 0.87 eV. Moreover, it is worthwhile noting that by increasing the superlattice parameter n up to 72, in our present work, we obtained a band gap of 1.51 eV, which is even closer to the experimental band gap of 1.48 eV reported in reference [1].) The insertion of the InAs monomolecular plane results in a reduction in the point group symmetry at each atomic site, and as a consequence almost all of the degenerate bands are split in figure 4(b). In contrast to the case for our *ab initio* results, the lower group of bands (in the energy range from -12.8 to -9.5 eV) in figure 4(b) are split as a result of the InAs insertion (but see the

DOS profile below). Our last remark about figure 4 is that the band gap for the $(GaAs)_5InAs$ structure is direct at the Γ point. This will be very useful in studying the variation of E_g versus the GaAs barrier thickness in the case where there is one inserted InAs monolayer and in that where there are two inserted InAs monolayers.

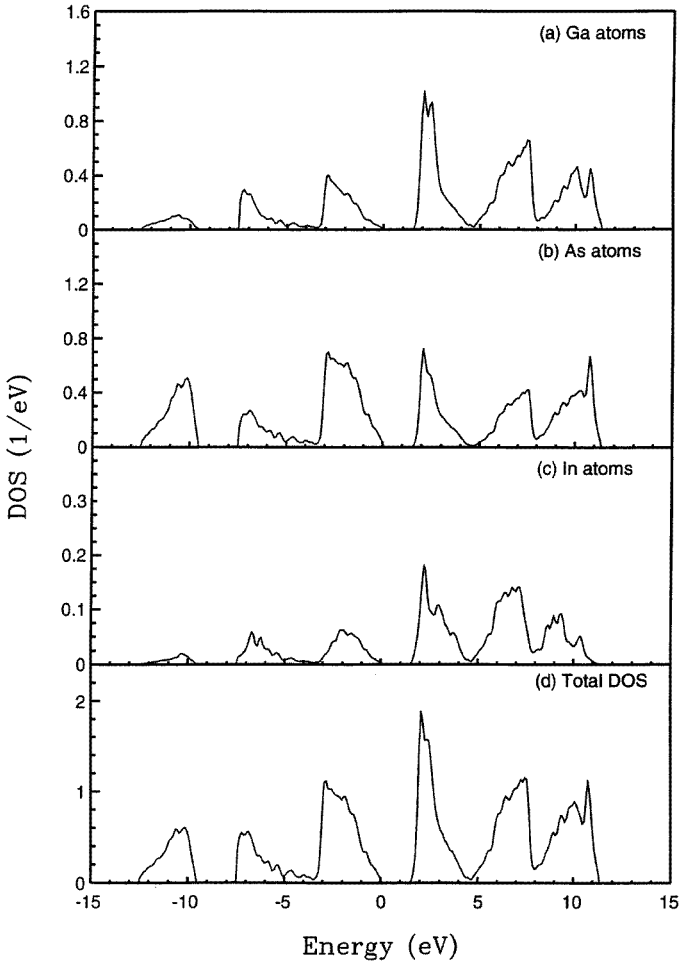

Figure 6. Partial density-of-states contributions from orbitals on (a) Ga atoms, (b) As atoms, and (c) In atoms to (d) the total density of states of a $(GaAs)_5InAs(001)$ SSL. The total DOS is normalized to ten electrons.

Figure 5 gives the corresponding densities of states, $N_0(E)$ and $N(E)$, for pure GaAs and the $(GaAs)_5InAs(001)$ SSL, respectively. It is worthwhile here to make the following remarks.

(i) Figure 5(c) reports the difference $\Delta N(E) = N(E) - N_0(E)$, in order to make evident the effects of the inserted InAs monomolecular plane. As seen in figure 5(c), the lowest group of bands is little affected by the insertion of the InAs plane, but to draw any conclusion one needs to study the partial/local density of states.

(ii) In figure 5(c), the peak at the bottom of the conduction band ($E \simeq 1.31$ eV) and the valley at the top of the valence band ($E \simeq 0$ eV) may suggest the localization of electrons

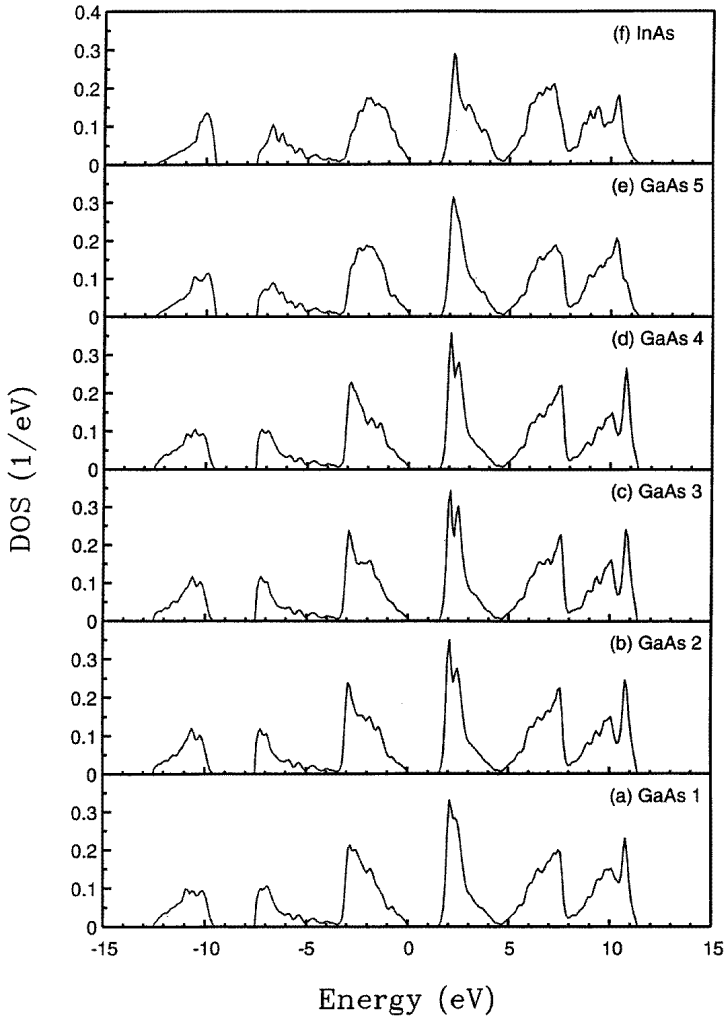

Figure 7. Local density-of-states contributions from each of the monolayers in the $(GaAs)_5InAs(001)$ strained superlattice. The sum of these DOS's should be equal to the total DOS normalized to ten electrons.

Table 2. The total charge density carried by each monolayer, presented in figure 7, and the corresponding ionicity. In the bulk, each zinc-blende molecule is assumed to possess eight electrons. The net charge is given in units of $-e$/molecule whereas the ionicity is expressed in units of e/molecule.

Monolayer	GaAs1	GaAs2	GaAs3	GaAs4	GaAs5	InAs
Net charge	8.075	7.996	7.994	7.996	8.075	7.864
Ionicity	-0.075	$+0.004$	$+0.006$	$+0.004$	-0.075	$+0.136$

and heavy holes respectively.

(iii) All other zigzag behaviour in figure 5(c) reflects the splitting of degenerate bands after the insertion of the InAs monolayer.

To study the structure of each of the three groups of bands, we display in figure 6 the partial DOS contributions and total DOS for the $(GaAs)_5InAs(001)$ SSL. The total DOS is normalized to ten electrons. The electronic structures of the cations (Ga and In) in figures 5(a) and 5(c) (respectively) reveal that they are electropositive atoms, because most of their DOS weights are in the CB (i.e., the integrated partial DOS up to the valence band edge is less than 4 electrons/atom). Moreover, the In atom is more electropositive than the Ga atom. Notice that the lowest group of bands has only small contributions coming from In atoms, and that is why it is less affected by the insertion of the InAs plane . (In fact, the eigenfunctions of this group of bands are distributed mainly over the s states of As atoms, as these states are the deepest in energy (see also the values of $E(\mathrm{s,a})$ in table 1).) Figure 6(c) shows that As is the most electronegative atom, because most of the weight of its local DOS is in the first group of bands and the valence band.

For the previous superlattice, we calculated the local DOS contributions from each monolayer to study the gap states, and the results are displayed in figure 7. It is worth making the following two remarks.

(i) First, the band gap for all of the layers in the $(GaAs)_5InAs(001)$ structure is the same ($E_g = 1.31$ eV) as that of the total DOS (figure 6(d)). This suggests that the gap states (electron and heavy-hole levels), related to InAs layer, have wavefunctions that extend considerably into the GaAs potential barriers, and that their overlap forms the minibands in this small-size superlattice.

(ii) The total charge of each monolayer can be calculated by integrating the corresponding local DOS up to the Fermi level (i.e. $q = \int_{E_{\min}}^{E_F} -2eN_l(E)\,\mathrm{d}E$, where $N_l(E)$ is the layer partial DOS, $E_{\min} = -15$ eV, E_F is the Fermi energy lying in the middle of the gap, $E_F = 0.65$ eV, and the number 2 is the spin degeneracy).

Assuming that the total charge of each monomolecular layer in the bulk is normalized to 8 electrons/molecule, the results, displayed in table 2, show the reliable changes in site occupancy due to the insertion of the InAs plane in the superlattice of figure 7. One can clearly see that drastic charge transfer occurs from the inserted InAs monolayer plane to the neighbouring GaAs planes. As shown in table 2, the total ionicity of the inserted InAs plane is found to be about $\Delta q = +0.136\,e$/molecule, where e is the absolute charge of the free electron. This, in turn, reveals the fact that the InAs plane, buried in GaAs, forms a type-I heterojunction. Last but not least, further analysis (descibed below) is still necessary to draw final conclusions about the nature of the gap states.

It is well known that GaInAs has a direct band gap at the Γ point over the whole range of solid composition (see figure 4(b)). Therefore, the energy gap as well as the localized levels can be calculated using just this latter $\boldsymbol{k}$-point. We performed the calculations on $(GaAs)_nInAs(001)$ superlattices, where n was varied up to 76. We have ascertained that there is only negligible variation of E_g if n increases above this latter value. We obtained $E_g = 1.510$ eV for $n = 76$. This yields the result that the energy gap of the InAs(GaAs) one-monolayer–host-crystal system is reduced by about 40 meV with respect to that of pure GaAs, in excellent agreement with the PL experiment. For the $(GaAs)_{76}InAs(001)$ superlattice, we have calculated the amplitude of the wavefunctions corresponding to the localized electron and heavy hole at the bottom of CB and top of VB respectively. In figure 8, the upper curve corresponds to electrons and the lower curve corresponds to holes. As seen in this figure, both electrons and holes are localized around the inserted InAs plane within a localization length of about 110 Å. These wavefunctions, plotted in figure 8, are mainly supported by the s, p_z, and s^* orbitals of atoms in the neighbourhood of the inserted InAs plane. Thus the exciton state is localized along the c-axis, and this explains the sharp

and intense PL peak and its polarization parallel to the plane. Moreover, as seen in figure 8, the inserted InAs monolayer is playing the role of a quantum well for all of the charge carriers, and this is, of course, consistent with the fact that GaAs/InAs forms a so-called type-I heterojunction when the GaAs is used as a substrate.

Figure 8. The calculated wavefunction amplitudes in the $(GaAs)_{76}InAs(001)$ superlattice, representing the InAs(GaAs) one-monolayer–host-crystal system. The upper curve corresponds to the electron state, while the lower curve represents the heavy-hole state.

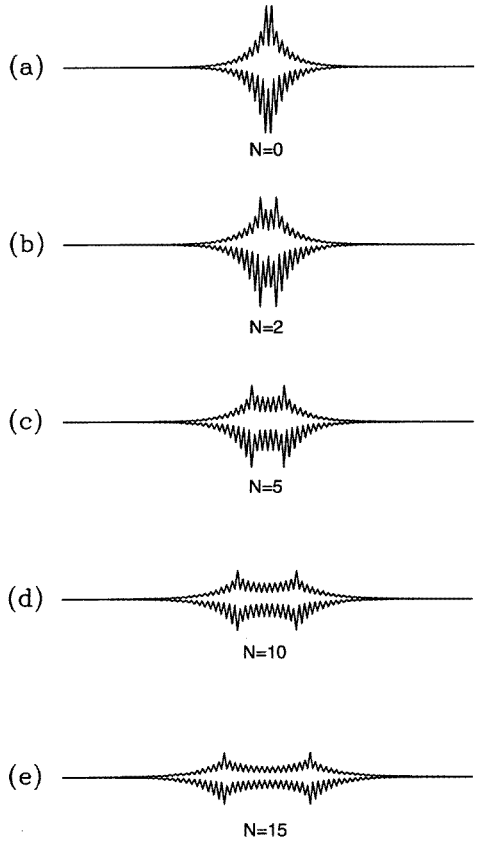

Figure 9. The calculated wavefunction amplitudes of the InAs(GaAs) two-monolayer–host-crystal system, where the InAs planes are separated by N monolayers of GaAs. The upper and lower curves correspond to the electron and heavy hole respectively. (a) The $N = 0$ case of two-monolayer-thick InAs in GaAs, (b) $N = 2$, (c) $N = 5$, (d) $N = 10$, and (e) $N = 15$.

We have also calculated the eigenenergies and eigenfunctions of the InAs(GaAs) two-monomolecular-plane–host-crystal system, where two InAs monolayers are separated by N monolayers of GaAs, using only the Γ point. More specifically, the calculation is performed on the $InAs/(GaAs)_N/InAs/(GaAs)_{75-N}$ superlattice with periodic boundary conditions.

We have chosen $N = 0$, 2, 5, 10, and 15 so as to allow a comparison with the PL experimental results of reference [3]. Our results for the band-gap energy E_g versus N are displayed in figure 10—see this figure and the discussion of it below. In figure 9, however, the eigenfunction amplitudes corresponding to the electron and heavy hole (gap levels) are displayed as upper and lower curves respectively. It can be easily seen in figure 9 that the degree of localization around the InAs monomolecular plane decreases as N increases. This behaviour is due to the increase in the confinement energies of the levels when the wells are further separated from each other. Of course, when N is large enough, the wells will be isolated, and the energy gap should have the same value, 1.51 eV, as that of the one-monolayer system.

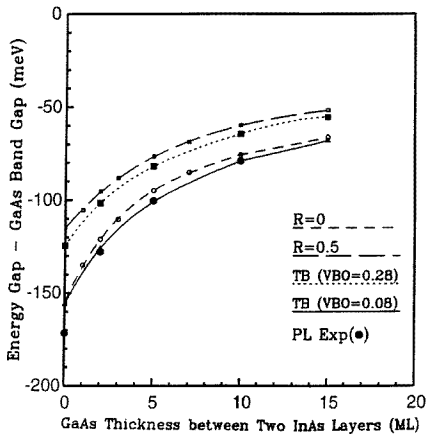

Figure 10. The energy gaps of the InAs(GaAs) two-monolayer–host-crystal system versus the barrier thickness, N. Solid circles (•) represent the PL peak photon energies of the samples grown by FME. The dotted and solid curves represent the results of our present sp^3s^* tight-binding calculations obtained using VBO = 0.28 and 0.08 eV respectively. The long- and short-dashed lines correspond to the results obtained using the finite-square-well model with replacement rates of $R = 0.5$ and $R = 0$ respectively.

In figure 10, our results for the energy gaps for the InAs(GaAs) two-monolayer–host-crystal system are expressed numerically as the difference from the pure GaAs band-gap energy, and are shown as solid and dotted curves corresponding to VBO = 0.08 and 0.28 eV respectively. The experimental results obtained by means of PL, measured at 2 K, from the work of Sato and Horikoshi [3], are shown as solid circles (•). The PL peak energies drastically increase with the distance between the InAs planes, especially when N is small, revealing that very sharp InAs monolayers were achieved using the FME growth technique. In an attempt to interpret the experimental results, Sato and Horikoshi [3] used a finite-square-well model which takes into account In–Ga replacement during growth. They studied the variation of E_g versus N as well as the replacement rate, R (which is defined as the ratio of the amount of In replacing Ga after one Ga monolayer has been supplied to the amount of In at the initial surface). They varied R from 0 to 0.98, but we show in figure 10 only two of their sets of results, corresponding to $R = 0$ and $R = 0.5$, for the purposes of comparison to our tight-binding results. Although the square-well model yielded energy gap results in good agreement with the PL experiments, it also relies on assumptions regarding the values of several parameters, such as the band discontinuities and effective masses of the charge carriers. (In the square-well model, the valence band

and conduction band discontinuities between strained InAs and GaAs were taken to be 0.4 and 0.6 eV respectively. The thickness of the InAs monolayer was taken to be 1.12 times as large as that of GaAs. The effective masses were taken to be $m_e = 0.0665m_0$ and $m_h = 0.34m_0$ for the electron and heavy hole, respectively, where m_0 denotes the free-electron mass, and to be the same in both the well and the barrier regions.) However, in our work, the valence band discontinuity was taken from our *ab initio* pseudopotential estimation [5] (VBO = 0.28 eV). Our results obtained using this VBO value, presented as a dotted curve, lie between the ones corresponding to replacement rates of $R = 0$ and $R = 0.5$. However, we note that our tight-binding results become even closer to the PL experimental data than the $R = 0$ curve when the VBO is decreased to about VBO = 0.08 eV (as shown by the solid line). Another discrepancy between our present work and the finite-square-well model is that, in our calculations, the InAs monolayer thickness is taken to be about 1.2 times as large as that of the GaAs monolayer, in order to preserve the In–As bulk bond length, as discussed in the introduction. Making this latter assumption appears to be more easily justifiable, as it is well supported by experimental observations [11]. Thus, it turns out that the use of the VBO value, obtained from the *ab initio* calculation, is the point to question in attempting to improve our tight-binding results to achieve a better fit to the PL data. This is, also, consistent with the fact that in the limit of an ultra-thin InAs layer in GaAs, the MTE breaks down, and the VBO could have a different value. Indeed, our results improved, and became even better than the square-well model with $R = 0$ when the VBO was decreased down to 0.08 eV, as is shown by the solid line in figure 10. Finally, we emphasize that the deviation of our theoretical results (solid curve) from the PL data in the case of a two-monolayer-thick InAs well ($N = 0$) may be attributed to some excitonic effect which is completely ignored in the calculation.

4. Conclusions

We have presented the calculated electronic structures of bulk GaAs, bulk InAs, and InAs(GaAs) monolayer–host-crystal systems using the sp^3s^* tight-binding model. The details of our calculations are described. Our results show that both electrons and holes are localized around the inserted InAs plane in the *c*-axis growth direction, and, therefore, this plane is playing the role of a quantum well for all of the charge carriers.

In the case of a InAs(GaAs) one-monolayer–host-crystal system, the energy gap is found to be about 40 meV smaller than that of bulk GaAs. The wavefunctions corresponding to the localized electron and heavy hole in the gap are found to be confined around the inserted InAs plane in the *c*-axis direction, and are mainly attributed to the s, p_z, and s^* orbitals of atoms in the neighbourhood of the plane. These results successfully explain the observed intense photoluminescence, and its polarization parallel to the plane.

However, for the case of the InAs(GaAs) two-monolayer–host-crystal system, where the two InAs planes are separated by N monolayers of GaAs, our results show that both electrons and holes are strongly localized around the two inserted InAs planes. The degree of localization increases as N becomes smaller, as a consequence of the decrease of the carrier confinement energies in the InAs quantum well. Our calculated band-gap energy versus N lies in between the PL experimental results and results for the finite-square-well model with the replacement rate $R = 0.5$. This is in the case where we took VBO = 0.28 eV, which was derived from our *ab initio* calculation [5]. Our results, however, get closer to the experimental data when the VBO is decreased to 0.08 eV. The variation of the VBO is legitimate, as an ultra-thin InAs layer is considered. Finally, the InAs(GaAs) monomolecular-plane–host-crystal system appears to be a promising structure as regards

band-gap engineering of lattice-mismatched heterostructures, and to have considerable potential as regards applications in high-speed and optoelectronic devices.

Acknowledgments

The author would like to thank Dr M Peressi for stimulating discussions, and Professor S Pantelides for the invitation to visit the Physics Department at Vanderbilt University, where this work was completed.

Appendix A

The bulk sp^3s^* Hamiltonian

The sp^3s^* tight-binding Hamiltonian in terms of the Löwdin basis set for the bulk fcc zinc-blende structure is given by

$$H = \begin{pmatrix} E_c & U_{ca} \\ U_{ac} & E_a \end{pmatrix}$$

where each element is a 5×5 matrix. The matrices E_c and E_a are diagonal, and represent the on-site energies of cations and anions respectively, whereas the 'hopping' terms U_{ca} and U_{ac} involve the transfer-matrix elements connecting orbitals on neighbouring sites. Of course, $U_{ac} = U_{ca}^{+}$, so the Hamiltonian is Hermitian. The elements of these matrices are

$$E_b = \begin{pmatrix} E(s,b) & 0 & 0 & 0 & 0 \\ 0 & E(p,b) & 0 & 0 & 0 \\ 0 & 0 & E(p,b) & 0 & 0 \\ 0 & 0 & 0 & E(p,b) & 0 \\ 0 & 0 & 0 & 0 & E(s^*,b) \end{pmatrix}$$

where b = 'c' or 'a' corresponding to cations or anions respectively, and

$$U_{ac} = \begin{pmatrix} V(s,s)g_0 & V(sa,pc)g_1 & V(sa,pc)g_2 & V(sa,pc)g_3 & 0 \\ -V(sc,pa)g_1 & V(x,x)g_0 & V(x,y)g_3 & V(x,y)g_2 & -V(pa,s^*c)g_1 \\ -V(sc,pa)g_2 & V(x,y)g_3 & V(x,x)g_0 & V(x,y)g_1 & -V(pa,s^*c)g_2 \\ -V(sc,pa)g_3 & V(x,y)g_2 & V(x,y)g_1 & V(x,x)g_0 & -V(pa,s^*c)g_3 \\ 0 & V(s^*a,pc)g_1 & V(s^*a,pc)g_2 & V(s^*a,pc)g_3 & 0 \end{pmatrix}$$

where the coupling to s^* states on different sites is omitted for simplicity [6], and we have

$$\begin{aligned} g_0(\boldsymbol{k}) &= \cos(\lambda_1)\cos(\lambda_2)\cos(\lambda_3) - \mathrm{i}\sin(\lambda_1)\sin(\lambda_2)\sin(\lambda_3) \\ g_1(\boldsymbol{k}) &= -\cos(\lambda_1)\sin(\lambda_2)\sin(\lambda_3) + \mathrm{i}\sin(\lambda_1)\cos(\lambda_2)\cos(\lambda_3) \\ g_2(\boldsymbol{k}) &= -\sin(\lambda_1)\cos(\lambda_2)\sin(\lambda_3) + \mathrm{i}\cos(\lambda_1)\sin(\lambda_2)\cos(\lambda_3) \\ g_3(\boldsymbol{k}) &= -\sin(\lambda_1)\sin(\lambda_2)\cos(\lambda_3) + \mathrm{i}\cos(\lambda_1)\cos(\lambda_2)\sin(\lambda_3) \end{aligned}$$

with $\lambda_1 = k_x a_L/4$, $\lambda_2 = k_y a_L/4$, and $\lambda_3 = k_z a_L/4$, where a_L is the lattice constant.

Appendix B

The superlattice sp^3s^* Hamiltonian

In the periodically repeated tetragonal supercell (001), each monatomic layer is represented by one atom. We assume that all of the constituents of the supercell are of zinc-blende type,

such as InAs(GaAs) systems. Then the Hamiltonian can be written in terms of the Löwdin basis set as

$$H = \begin{pmatrix} \ddots & \ddots & \ddots & & & & & \\ & V_{\mathrm{ca}} & E_{\mathrm{c}} & U_{\mathrm{ca}} & & & & \\ & & U_{\mathrm{ac}} & E_{\mathrm{a}} & V_{\mathrm{ac}} & & & \\ & & & V_{\mathrm{ca}} & E_{\mathrm{c}} & U_{\mathrm{ca}} & & \\ & & & & U_{\mathrm{ac}} & E_{\mathrm{a}} & V_{\mathrm{ac}} & \\ & & & & & \ddots & \ddots & \ddots \end{pmatrix}$$

where each element is a 5×5 matrix. The matrices E_{b} are defined in appendix A, where b = 'a' or 'c' corresponding to the on-site energies of anions or cations respectively. It is also understood that the 'hopping' terms have the properties $U_{\mathrm{ca}} = U_{\mathrm{ac}}^{+}$ and $V_{\mathrm{ac}} = V_{\mathrm{ca}}^{+}$, because the Hamiltonian is Hermitian. The elements of the matrices U_{ac} and V_{ca} are

$$U_{\mathrm{ac}} = \begin{pmatrix} V(\mathrm{s,s})g_{0u} & V(\mathrm{sa,pc})g_{1u} & V(\mathrm{sa,pc})g_{2u} & V(\mathrm{sa,pc})g_{3u} & 0 \\ -V(\mathrm{sc,pa})g_{1u} & V(\mathrm{x,x})g_{0u} & V(\mathrm{x,y})g_{3u} & V(\mathrm{x,y})g_{2u} & -V(\mathrm{PS})g_{1u} \\ -V(\mathrm{sc,pa})g_{2u} & V(\mathrm{x,y})g_{3u} & V(\mathrm{x,x})g_{0u} & V(\mathrm{x,y})g_{1u} & -V(\mathrm{PS})g_{2u} \\ -V(\mathrm{sc,pa})g_{3u} & V(\mathrm{x,y})g_{2u} & V(\mathrm{x,y})g_{1u} & V(\mathrm{x,x})g_{0u} & -V(\mathrm{PS})g_{3u} \\ 0 & V(\mathrm{s^*a,pc})g_{1u} & V(\mathrm{s^*a,pc})g_{2u} & V(\mathrm{s^*a,pc})g_{3u} & 0 \end{pmatrix}$$

where, in the last column, (PS) stands for (pa, s*c), and

$$g_{0u}(\boldsymbol{k}) = \frac{1}{4}\left[\exp(k_x A_x/2 + k_z A_z) + \exp(-k_x A_x/2 + k_z A_z)\right]$$

$$g_{1u}(\boldsymbol{k}) = \frac{1}{4}\left[\exp(k_x A_x/2 + k_z A_z) - \exp(-k_x A_x/2 + k_z A_z)\right]$$

and $g_{2u}(\boldsymbol{k}) = g_{1u}(\boldsymbol{k})$, and $g_{3u}(\boldsymbol{k}) = g_{0u}(\boldsymbol{k})$, and

$$V_{\mathrm{ca}} = \begin{pmatrix} V(\mathrm{s,s})g_{0v} & -V(\mathrm{sc,pa})g_{1v} & -V(\mathrm{sc,pa})g_{2v} & -V(\mathrm{sc,pa})g_{3v} & 0 \\ V(\mathrm{sa,pc})g_{1v} & V(\mathrm{x,x})g_{0v} & V(\mathrm{x,y})g_{3v} & V(\mathrm{x,y})g_{2v} & V(\mathrm{SP})g_{1v} \\ V(\mathrm{sa,pc})g_{2v} & V(\mathrm{x,y})g_{3v} & V(\mathrm{x,x})g_{0v} & V(\mathrm{x,y})g_{1v} & V(\mathrm{SP})g_{2v} \\ V(\mathrm{sa,pc})g_{3v} & V(\mathrm{x,y})g_{2v} & V(\mathrm{x,y})g_{1v} & V(\mathrm{x,x})g_{0v} & V(\mathrm{SP})g_{3v} \\ 0 & -V(\mathrm{pa,s^*c})g_{1v} & -V(\mathrm{pa,s^*c})g_{2v} & -V(\mathrm{pa,s^*c})g_{3v} & 0 \end{pmatrix}$$

where, in the last column, (SP) stands for (s*a, pc), and

$$g_{0v}(\boldsymbol{k}) = \frac{1}{4}\left[\exp(-k_y A_y/2 + k_z A_z) + \exp(k_y A_y/2 + k_z A_z)\right]$$

$$g_{1v}(\boldsymbol{k}) = \frac{1}{4}\left[-\exp(-k_y A_y/2 + k_z A_z) + \exp(k_y A_y/2 + k_z A_z)\right]$$

$$g_{2v}(\boldsymbol{k}) = \frac{1}{4}\left[\exp(-k_y A_y/2 + k_z A_z) - \exp(k_y A_y/2 + k_z A_z)\right]$$

$$g_{3v}(\boldsymbol{k}) = \frac{1}{4}\left[-\exp(-k_y A_y/2 + k_z A_z) - \exp(k_y A_y/2 + k_z A_z)\right]$$

with $A_x = A_y = a_{\mathrm{L}}/\sqrt{2}$, where a_{L} is the lattice constant of GaAs and A_z is the distance from the layer of cations c to the upper layer of anions a (we denote this interplane distance by $a_{\perp}$(XAs)). For example, in the case of Ga atoms $a_{\perp}$(GaAs) = 1.41 Å, whereas in the case of In atoms, $a_{\perp}$(InAs) = 1.695 Å.

References

[1] Sato M and Horikoshi Y 1989 *J. Appl. Phys.* **66** 851
[2] Sato M and Horikoshi Y 1991 *J. Appl. Phys.* **69** 7697
[3] Sato M and Horikoshi Y 1992 *Surf. Sci.* **267** 195
[4] Tit N and Peressi M 1995 *Phys. Rev.* B **52** 10 776
[5] Tit N, Peressi M and Baroni B 1993 *Phys. Rev.* B **48** 17 607
[6] Vogl P, Hjalmarson H P and Dow J D 1983 *J. Phys. Chem. Solids* **44** 365
[7] Chelikowsky J R and Cohen M L 1976 *Phys. Rev.* B **14** 556
[8] *Landolt–Börnstein New Series (Numerical Data and Functional Relationships in Science and Technology)* 1982 Group III, ed O Madelung (Berlin: Springer)
[9] Priester C, Allan G and Lannoo M 1988 *Phys. Rev.* B **37** 8519
[10] Harrison W 1980 *Electronic Structure and the Properties of Solids* (San Francisco, CA: Freeman) ch 6
[11] Brandt O, Ploog K, Bierwolf R and Hohenstein M 1992 *Phys. Rev. Lett.* **68** 1339
[12] Löwdin P O 1950 *J. Chem. Phys.* **18** 365
[13] Cullum J K and Willoughby R A 1985 *Theory (Lanczos Algorithm for Large Eigenvalue Computations 1)* (Birkhäuser: Basel)
[14] Wu Yi-hong, Fujita S and Fujita S 1990 *J. Appl. Phys.* **67** 908
[15] Wang C Z and Callaway J 1978 *Comput. Phys. Commun.* **14** 327